JGP
The Journal of General Physiology
Vol 133 • No 5 • May 2009

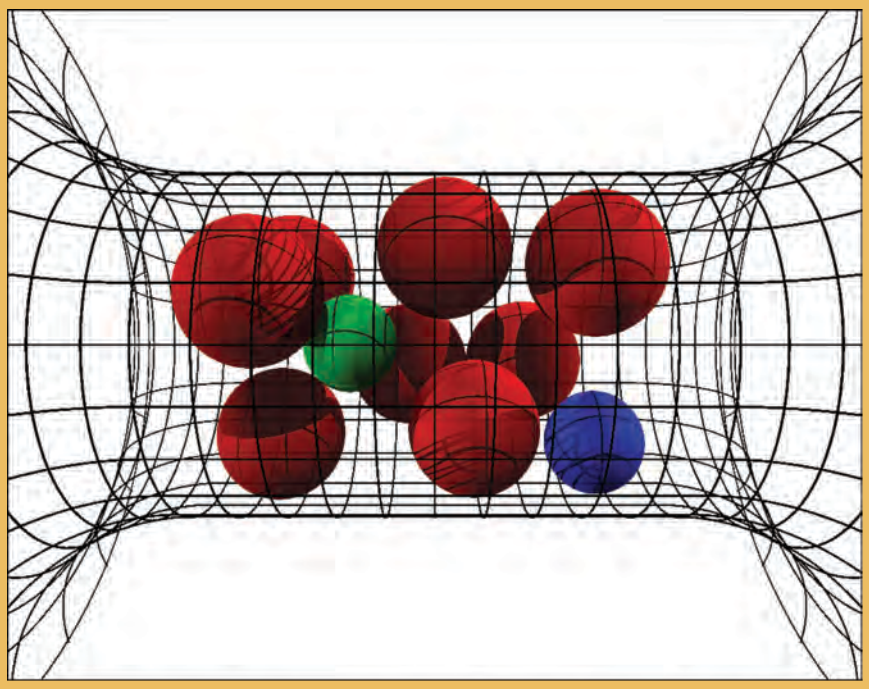

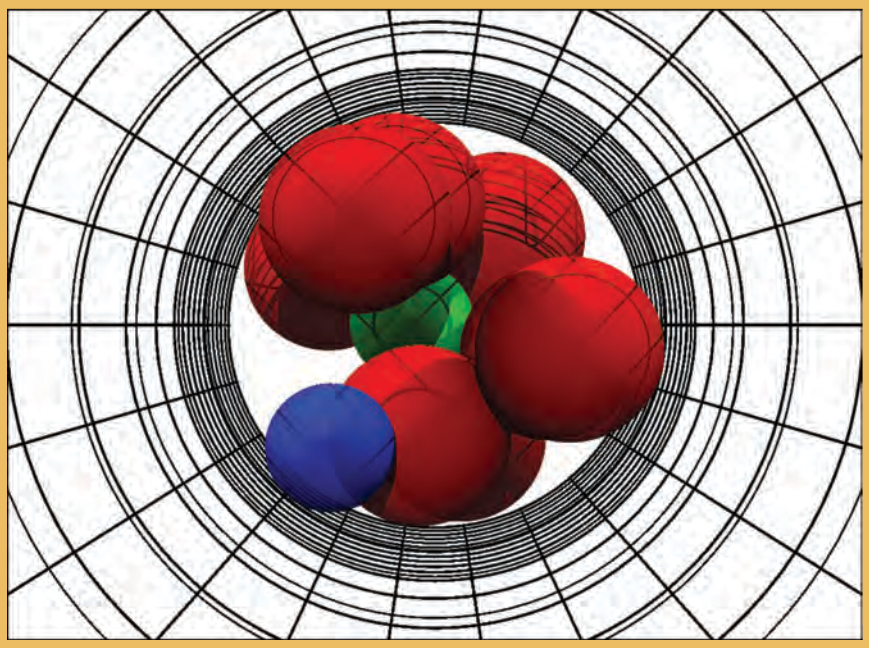

www.jgp.org

Published April 27, 2009

Ionic selectivity in L-type calcium channels by electrostatics and hard-core repulsion

Dezső Boda,[1,2] Mónika Valiskó,[1] Douglas Henderson,[2] Bob Eisenberg,[3] Dirk Gillespie,[3] and Wolfgang Nonner[4]

[1]Department of Physical Chemistry, University of Pannonia, H-8201 Veszprém, Hungary
[2]Department of Chemistry and Biochemistry, Brigham Young University, Provo, UT 84602
[3]Department of Molecular Biophysics and Physiology, Rush University Medical Center, Chicago, IL 60612
[4]Department of Physiology and Biophysics, Miller School of Medicine, University of Miami, Miami, FL 33101

A physical model of selective "ion binding" in the L-type calcium channel is constructed, and consequences of the model are compared with experimental data. This reduced model treats only ions and the carboxylate oxygens of the EEEE locus explicitly and restricts interactions to hard-core repulsion and ion–ion and ion–dielectric electrostatic forces. The structural atoms provide a flexible environment for passing cations, thus resulting in a self-organized induced-fit model of the selectivity filter. Experimental conditions involving binary mixtures of alkali and/or alkaline earth metal ions are computed using equilibrium Monte Carlo simulations in the grand canonical ensemble. The model pore rejects alkali metal ions in the presence of biological concentrations of Ca^{2+} and predicts the blockade of alkali metal ion currents by micromolar Ca^{2+}. Conductance patterns observed in varied mixtures containing Na^+ and Li^+, or Ba^{2+} and Ca^{2+}, are predicted. Ca^{2+} is substantially more potent in blocking Na^+ current than Ba^{2+}. In apparent contrast to experiments using buffered Ca^{2+} solutions, the predicted potency of Ca^{2+} in blocking alkali metal ion currents depends on the species and concentration of the alkali metal ion, as is expected if these ions compete with Ca^{2+} for the pore. These experiments depend on the problematic estimation of Ca^{2+} activity in solutions buffered for Ca^{2+} and pH in a varying background of bulk salt. Simulations of Ca^{2+} distribution with the model pore bathed in solutions containing a varied amount of Li^+ reveal a "barrier and well" pattern. The entry/exit barrier for Ca^{2+} is strongly modulated by the Li^+ concentration of the bath, suggesting a physical explanation for observed kinetic phenomena. Our simulations show that the selectivity of L-type calcium channels can arise from an interplay of electrostatic and hard-core repulsion forces among ions and a few crucial channel atoms. The reduced system selects for the cation that delivers the largest charge in the smallest ion volume.

INTRODUCTION

Voltage-dependent calcium channels relay electrical signals from the cell membrane to the cytoplasm by allowing extracellular Ca^{2+} to flow into the cell, where Ca^{2+} acts as a chemical signal (Hagiwara, 1983; Hille, 2001). The Ca^{2+}-conducting pore of these transmembrane proteins selects Ca^{2+} over the much more abundant cations Na^+ and K^+. Four amino acid residues bearing acidic side chains (the "EEEE" locus in L-type calcium channels) extend into this pore, and all cooperate in selecting Ca^{2+} with high affinity (Yang et al., 1993; Ellinor et al., 1995; Chen et al., 1996; Koch et al., 2000; for review see Sather and McCleskey, 2003). Here, we compute consequences of a physical model of selectivity in which ions compete for interaction with negative structural charge and for restricted space in the EEEE locus.

In physiological solutions containing 2 mM Ca^{2+} and 100–150 mM Na^+, the L-type channel conducts a relatively small current carried by Ca^{2+}. When Ca^{2+} is left out of the solutions (and Ca^{2+} contaminants are chelated), the channel conducts a large current carried by Na^+. A key observation in calcium channel selectivity has been the "anomalous mole fraction effect" (Kostyuk et al., 1983; Almers et al., 1984; Almers and McCleskey, 1984; Hess and Tsien, 1984). When the external bath includes 30–150 mM Na^+ and micromolar Ca^{2+}, currents through the channel are smaller than the currents carried in solutions containing only Na^+ (with zero Ca^{2+}) and the currents carried in physiological solutions (containing millimolar Ca^{2+}). Almers and McCleskey (1984) proposed "that Ca^{2+} channels, being innately permeable to all physiological inorganic cations, derive their Ca^{2+} selectivity from high-affinity Ca^{2+}-binding sites located within the aqueous pore, and that these sites represent normal way stations for Ca^{2+} during permeation." In this view, the channel contains Ca^{2+} when the bath contains tiny concentrations of Ca^{2+}. A tiny concentration of Ca^{2+} in mixed solutions containing Na^+ reduces current a great deal.

Correspondence to Wolfgang Nonner: wnonner@med.miami.edu

Abbreviations used in this paper: CSC, charge/space competition; ICC, induced charge computation; MC, Monte Carlo.

The Rockefeller University Press $30.00
J. Gen. Physiol. Vol. 133 No. 5 497–509
www.jgp.org/cgi/doi/10.1085/jgp.200910211

Published April 27, 2009

That tiny concentration of Ca^{2+} does not allow a detectable Ca^{2+} current to flow. Under physiological ionic conditions, the channel is selective for Ca^{2+} because the preferential absorption of Ca^{2+} into the channel more than compensates for the smaller concentration of Ca^{2+} in the bath.

Experimental studies of calcium channel selectivity have been extended to other alkaline earth and alkali metal cations so the effects of both ion size and charge can be studied (Ca^{2+} and Na^+ have different charges but nearly identical crystal radii). Studies with the other ions are confusing. Exactly opposite selectivity sequences are obtained depending on how the cations are presented to the channel. The magnitude of the conductance for a species in solutions containing just that species shows selectivity for large and monovalent cations: $Cs^+ > K^+ > Na^+ > Li^+ > Ba^{2+} > Ca^{2+}$. On the other hand, when two or more cation species are simultaneously present in the bathing solutions, the channel preferentially conducts the opposite way. In mixed solutions, the channel prefers small and divalent cations: $Ca^{2+} > Ba^{2+} > Li^+ > Na^+ > K^+ > Cs^+$ (Reuter and Scholz, 1977; Fenwick et al., 1982; Lee and Tsien, 1984; Hess et al., 1986).

We interpret the results this way. When the baths contain one species, the channel contains that species and conducts it at a rate determined by the friction that the species has against the channel. On the other hand, when the baths contain two species, the extent of absorption into the channel determines which species carries current. The two or more species compete for conduction by competing for occupancy of the channel. Here, we are concerned with the physical basis of the competition for occupancy because that appears to control physiological selectivity.

An important class of experiments concerns mixed solutions in which all the cations have the same charge. Substantial selectivity is detected. A small mole fraction of Li^+ in a Na^+/Li^+ mixture reduces channel conductance toward the level found in the pure solution of Li^+ (containing no Na^+) (Prod'hom et al., 1989); a similar effect of Ca^{2+} is observed in Ba^{2+}/Ca^{2+} mixtures (Almers and McCleskey, 1984; Lansman et al., 1986; Friel and Tsien, 1989; Yue and Marban, 1990).

When ions have different charges, different behavior is reported. Selectivity with regard to monovalent cations appears to be absent in mixed solutions containing the divalent cation, Ca^{2+}. Here, the same small concentrations of Ca^{2+} (≈1 μM) reduce the currents carried by Na^+, Li^+, and K^+ (Hess and Tsien, 1984; Lansman et al., 1986; Pietrobon et al., 1988; Kuo and Hess, 1993a,b; Yang et al., 1993). The effect of Ca^{2+} in mixed solutions with Na^+ is much the same whether they contain 30 or 150 mM Na^+ (Kostyuk et al., 1983; Almers and McCleskey, 1984; Hess and Tsien, 1984).

Carboxylate groups like those of the EEEE locus of L-type Ca channels coordinate Ca^{2+} in many proteins (Dudev and Lim, 2004). Carboxylates chelate Ca^{2+} in organic compounds used as Ca^{2+} buffers or indicators. Because Ca^{2+} selectivity arises in so many different structures—channels, proteins, and relatively small organic anions—that have only a few crucial atoms in common, we try to construct a model of selectivity that includes only those common atoms. We construct a reduced model of a Ca^{2+} "binding site," trying to identify physical interactions that are common and essential to all. When the structure of this channel is measured, comparison with this simple model will test the model and reveal the special properties produced by the special structure of the real channel.

A reduced model of the EEEE locus has been proposed by Nonner et al. (2000) and has been developed using theoretical analysis and simulation (Boda et al., 2000, 2001, 2002b, 2006, 2007b; Nonner et al., 2001; Gillespie et al., 2002, 2005; Gillespie, 2008). In this model, the charged groups of the EEEE locus form part of the liquid that fills the selectivity filter. Selectivity is produced by the competition between attraction and repulsion (Henderson, 2009). Selectivity comes from the balance of the attractive Coulombic interaction of the ions and structural charged groups in the filter and the repulsive excluded volume of the ions and structural groups in the small volume of the filter.

Cations are electrostatically attracted by this selectivity filter, but, because of the small volume of the filter and the excluded volume of the ions and structural charged groups, small and divalent cations are more effective in balancing the negative structural charge of the filter (a Ca^{2+} ion delivers twice the charge of a Na^+ ion in about the same particle volume). This mechanism of selectivity has been called charge/space competition (CSC). A calcium channel model in which the charges of the EEEE locus are embedded in a solid pore wall has been proposed by Corry et al. (2001); this model has difficulty producing strong Ca^{2+} binding under physiological conditions (Boda et al., 2008). The CSC model has been extended to the DEKA locus of sodium channels, which select for small monovalent cations ($Li^+ > Na^+ > K^+ > Cs^+$) (Boda et al., 2002a, 2007a). A reduced model has also been studied for the selectivity filter of potassium channels (Noskov and Roux, 2007).

In this study, we compute the consequences of the CSC model for a broad variety of ionic conditions in which L-type calcium channels have been experimentally tested. Our purpose is to see to what extent the physics included in the model can produce patterns of ion "binding" that the experiments have revealed. We discuss structures that emerge in our particle simulations and relate them to the barrier-and-well landscape inferred from chemical–kinetics models. We point out a potential problem in the use of Ca^{2+} buffers in varied backgrounds of alkali metal ion that is relevant for the interpretation of some of these experiments.

Published April 27, 2009

MATERIALS AND METHODS

Model

In our model, most of the unknown atomic structure of the calcium channel is reduced to a coarse-grained geometry (Fig. 1 A). The protein matrix, represented as a continuum solid with dielectric coefficient $\varepsilon_p = 10$, forms an aqueous pore that interconnects the two baths. Water in the baths and pore is described in the "primitive model"; that is, as an implicit solvent that is a continuum dielectric with uniform dielectric coefficient ε_W. In our case, $\varepsilon_w = 80$. The central part of the pore, a cylinder with radius $R = 3.5$ Å and length $L = 10$ Å ("selectivity filter"), includes the only atoms of the protein that are described in an explicit, although reduced, fashion. These atoms are eight "oxygen ions," each with the charge $-1/2\ e$ (Fig. 1, B and C, red spheres). They represent the charged terminal atoms of the four glutamate residues of the EEEE locus. The structural oxygen ions are confined to the selectivity filter by a hard-wall potential; they cannot overlap any boundary of the cylinder but are unrestricted to move within their confined space; thus, their centers are confined in the region $r \leq 2.1$ Å, $|z| \leq 3.6$ Å. The oxygen ions can "coordinate" counterions as particles of a confined liquid; their arrangement in Fig. 1 (B and C) represents one snapshot of the various configurations during a simulation. The oxygen ions are not tethered together in pairs in this reduced model.

The ions of the electrolyte are modeled as charged hard spheres with crystal radii (see legend of Fig. 1). These ions are restricted to the aqueous space of the model by hard walls. Fig. 1 A shows only the small central region of the simulation cell. The entire simulation cell is a cylinder, with typical radius of 64 Å and length of 300 Å. Depending on the bath concentrations of the ions in the particular simulation, the total number of cations present at a time in the simulation cell is ≈100–300. The "membrane" region, in which the channel is imbedded, excludes ions by hard walls but is assigned the same dielectric coefficient as the aqueous space (rather than a lipid-like dielectric coefficient). This choice of membrane dielectric coefficient reduces the amount of computation for the electrostatics with no significant effects on the simulation results (Boda et al., 2006).

Method of simulation

Monte Carlo (MC) simulations using Metropolis sampling are performed in the grand canonical ensemble (Valleau and Cohen, 1980) that allows efficient computation with very small ionic concentrations, such as those important for calcium channels. In this ensemble, the temperature, volume, and the chemical potentials of particles are constant. Our methods of sampling (including their acceptance tests) have been described previously (Boda et al., 2002b, 2006, 2008). Attempts to move a particle in this study consist of: (1) small changes from the old position (for sampling of regions with the high densities characteristic of condensed phases, i.e., liquids; this is the only kind of attempt used for the oxygen ions in the selectivity filter); (2) changes to a new position selected randomly from a uniform distribution anywhere in the cell (for sampling regions with gas-like densities, e.g., our implicit–solvent model of ionic solutions); (3) moving a particle from a position in the selectivity filter to a position in the baths, or vice versa; this is a preferential move between subvolumes and thus the acceptance test includes a factor for the subvolume ratio to prevent statistical bias (Boda et al., 2002b); (4) insertion or removal of a neutral group of ions (e.g., $Na^+ + Cl^-$ or $Ca^{2+} + 2Cl^-$) into or from the simulation cell; and (5) particle insertions or deletions analogous to (4) but involving subvolumes of the simulation cell (in particular, the selectivity filter) (Boda et al., 2008). Only cation insertions or deletions are applied in these subvolumes; Cl^- ions are still inserted into, or deleted from, the whole simulation cell. Attempts (4) and (5) maintain constant chemical potentials without disturbing the total electric charge of the system and thus establish the grand canonical ensemble. The preference sampling types (3) and (5) are essential for rapid convergence when some ion species (like Ca^{2+}) are present in very small bath concentrations and are also found in large concentrations in small parts of the simulation cell.

In the grand canonical ensemble, the chemical potentials of ions are chosen and bath concentrations are computed by the simulation. We determine chemical potentials needed to establish prescribed bulk concentrations of the bath solution by an iteration in a separate grand canonical ensemble simulation (Malasics et al., 2008); this simulation, unlike the simulations with the channel system, uses a large cubic cell with periodic boundary conditions. We report the prescribed bulk concentrations rather than the chemical potentials that are required to establish them in the grand canonical ensemble.

The acceptance tests of new particle configurations involve the total electrostatic energy of a configuration. Charge interactions occur in our system not only between ions (including structural ions), but also between ions and charges induced by the ions in the dielectrics. Because spatial transitions between dielectrics are sharp (i.e., discontinuous) in our model, the induced charges are boundary charges. These are computed using a boundary element method that we have called "induced charge computation" (ICC) (Boda et al., 2004, 2006). The surface discretization for solving the boundary integral equation is shown for the pore wall in Fig. 1 (B and C). For a given dielectric model, the coefficient matrix produced by the discretized integral equation does not depend on the ion configuration. It is inverted at the beginning of the simulation. Vectors of discretized induced charge for varied ion configurations are computed thereafter by a matrix–vector multiplication. The computational efficiency of this method is essential for our simulations because it is efficient enough to allow the total electrostatic interaction to be computed for each attempted move that does not generate particle–particle or particle–wall overlap. The ICC method thereby allows us to solve the simulated system self-consistently. The accuracy of the ICC method has been tested (Boda et al., 2006).

The presented simulation results are averages of many runs performed on multiple processors and starting from different seed configurations. An average comprises 6×10^8 to 1.2×10^9 MC attempts.

Computation of pore conductance

MC simulations provide spatial density distributions of ions at thermodynamic equilibrium. Experiments measure ionic current flowing under a thermodynamic driving force. To relate simulation results to experiment, we include density distributions, computed by simulation, into an estimate of slope conductance γ obtained in the limit of small driving force. We describe ion transport as drift-diffusion in a gradient of chemical potential:

$$-\mathbf{J}_i(\mathbf{r}) = \frac{D_i(\mathbf{r})}{k_B T}\rho_i(\mathbf{r})\nabla\mu_i(\mathbf{r}), \tag{1}$$

where $\mathbf{J}_i(\mathbf{r})$ is the flux density of species i at location $\mathbf{r}$, D_i the generally location-dependent diffusion coefficient of the species, k_B the Boltzmann constant, T the absolute temperature, ρ_i the number density of the species, and μ_i the chemical potential of the species. The chemical potential includes the "concentration" term of the ideal gas, the "excess" term accounting for the interactions of an ion with other ions and the channel, and the term due to the external electric field acting on the ions (if it is present, as in a voltage clamp experiment).

We focus on the conductance γ of the ion-selective part of the model pore, the cylinder of radius R and length L that confines the oxygen ions (Fig. 1), and ignore resistance in the wider parts

Published April 27, 2009

of the model pore and the baths. When a small driving force is applied between the flat surfaces of the cylinder, the local perturbations of the chemical potential with regard to the uniform chemical potential established in equilibrium will be small (in particular in the radial dimension in which no gradient is applied). We therefore approximate the chemical potential as uniform over a cross section of the cylinder. Because our simulations do not compute the diffusion coefficient, we assume that the diffusion coefficient is uniform in the cylinder. With these approximations, Eq. 1 yields for the total flux J_i^T of species i through the pore:

$$-J_i^T = \frac{D_i}{k_B T}\frac{d\mu_i(z)}{dz}\int_0^R \rho_i(r,z)2\pi r dr = \frac{D_i}{k_B T}\frac{d\mu_i(z)}{dz}n_i(z), \qquad (2)$$

where $n_i(z)$ is the axial number density of ions (number per unit pore length) at axial location z. When the solutions bathing the ends of the filter region are symmetrical and contain several ionic species of charge $z_i e_0$, and an exceedingly small voltage ∂V is applied across the system, the total conductance γ of the pore is:

$$\gamma = e_0\sum_i z_i \left.\frac{\partial J_i^T}{\partial V}\right|_{V_{L/2}-V_{-L/2}=0} = \sum_i D_i \frac{z_i^2 e_0^2}{k_B T}\left(\int_{-L/2}^{L/2}\frac{dz}{n_i(z)}\right)^{-1}. \qquad (3)$$

The axial ionic densities n_i are computed from MC simulation results. The diffusion coefficient for each species is an external parameter. It is chosen to produce the experimental pore conductance determined in the presence of a single cation species. Conductances with mixed solutions are predicted using the pure-solution values of diffusion coefficients.

It is important to note that the assumption of uniformity in the cross section of the pore that is made here for the chemical potential does not imply that other variables, such as the spatial number density of ions or the mean electric potential, be uniform. In fact, our simulations show substantial non-uniformity of the equilibrium ionic densities in the radial dimension (Boda et al., 2006, 2007a,b). Our estimate of pore conductance only requires approximate uniformity of the chemical potential.

These approximations and equations establish the slope conductance γ and the size (i.e., "scale") of the current through the channel. They do not capture nonlinear effects that might occur when large voltages or concentration gradients are applied. The concentration profiles we compute under equilibrium conditions are obtained with simulations using self-consistent electrostatics. When the system is nonequilibrium, the concentration profiles would have to be recalculated to be self-consistent. The nonequilibrium effects on potential profiles underlie much of the interesting behavior of devices described approximately by the drift-diffusion and adjoined Poisson equations (Selberherr, 1984; Jacoboni and Lugli, 1989; Eisenberg, 1996a,b, 2005; Lundstrom, 2000).

RESULTS

We study the consequences of a CSC model of the L-type calcium channel (Boda et al., 2007b). Using MC simulations in the grand canonical ensemble, we directly compute ion distributions inside a channel that links baths containing mixtures of ionic species, some at very low concentrations. In this reduced model of the channel, structural ions of the EEEE locus and free ions interact in the pore like the particles of a highly concentrated, confined electrolyte solution. The free and structural ions are described as charged hard spheres, with the solvent and protein matrix represented by continuum dielectrics. The electrostatics of the system are computed for each attempted move of a free or structural ion. These simulations are computationally efficient for exploring many ionic conditions of interest self-consistently and with small statistical error.

When in the following we compare predictions of the model and experimental data, we use one and the same model (Fig. 1), without changing any parameters. Experimental data used here necessarily were measured from L-type calcium channels from different tissues and species of animal, which presumably include a variety of (sub)types of the channel.

Selective absorption of cations with equal charges

The L-type calcium channel selects for Ca^{2+} over Na^+ and K^+ in physiological solutions. The channel also selects among ions of the same charge, both monovalent or divalent. Our model describes ions as charged hard spheres. Besides charge, the model pore can distinguish ions only by their radius (we use crystal radii; see legend of Fig. 1). Our model and simulations include no other kinds of energy, e.g., energy arising from changes in shape of electron orbitals, hydrogen bonds, etc. The question is, To what extent can such a model then account for distinctions made by real channels among ions of the same charge?

We simulate an experiment in which two ion species (Na^+ and K^+, or Ca^{2+} and Ba^{2+}) are present in bulk solutions in different mole fractions with the same fixed total concentration. As always in our equilibrium simulations, both baths contain the same solutions. We use these two pairs of ion species because the ionic radii of Na^+ and Ca^{2+} are similar, as are those of K^+ and Ba^{2+}. A comparison can be made of the effects of ion size in two systems, one with monovalent ions and the other with divalent ions. Fig. 2 shows axial profiles of computed ion concentrations for different mole fractions.

In the profiles of Fig. 2, cations are most concentrated (1) at or near the axial center of the pore and (2) just beyond the structural oxygen ions. Packing constraints corresponding to the different radii of the ions produce differences in the spacing of the concentration peaks. The central region concentration of the small ions has a divided peak, but that of the large ions has a single, broad maximum. The peripheral concentration peaks tend to be larger for the larger ions than for the smaller ions, as if the central region of the pore is less accessible to the larger ions. If larger ions are less able to enter the central region of the pore, they must screen the structural charges from more remote locations, from the peripheral regions where these larger ions can fit more easily. Size selectivity of the model pore is shown by the mole fractions required to produce similar amounts of ion in the central 5 Å of the pore: mole fractions of 0.95 for the larger ions are required for approximately equal concentrations of ions in the pore. The profiles depend

Published April 27, 2009

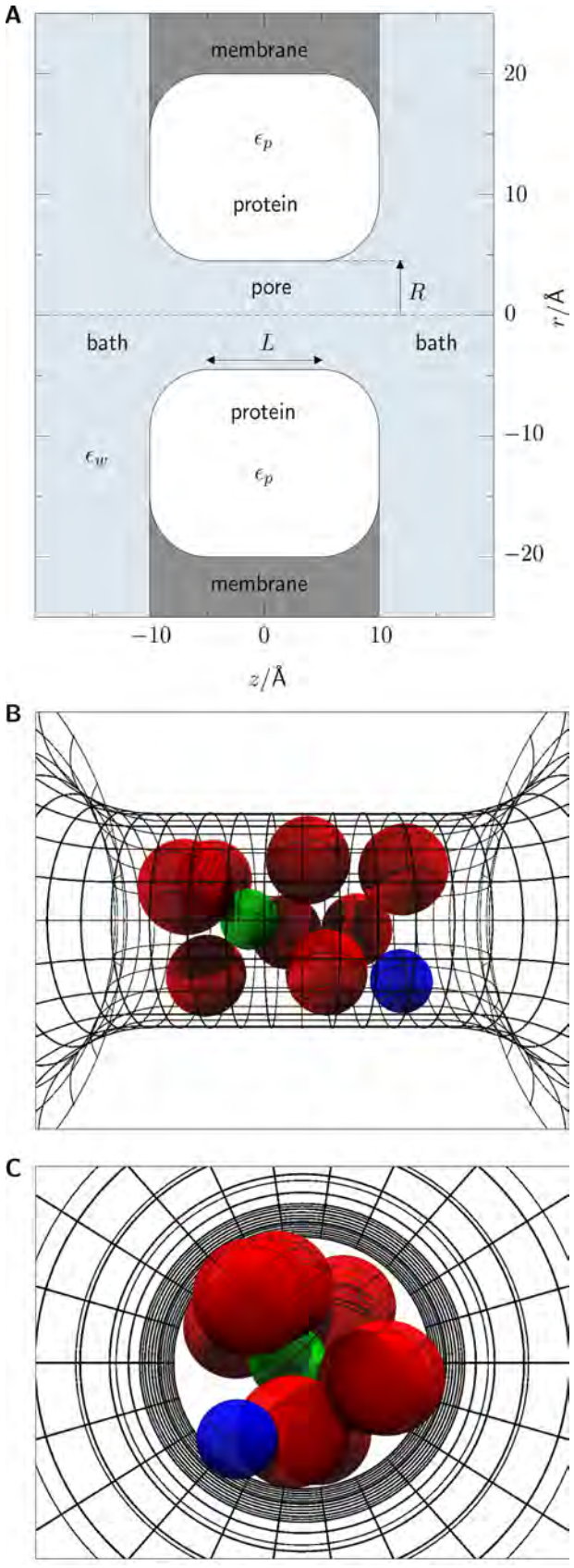

Figure 1. Geometry of the model. (A) Axial cross section through the central region of the cylindrical simulation cell containing the pore. The selectivity filter is the central pore region (R = 3.5 Å, L = 10 Å) confining the oxygen ions of the EEEE locus. The dielectric coefficients are ε_w = 80 (aqueous regions, light gray) and ε_p = 10 (protein and membrane regions, white and dark gray). (B and C) Spatial views of the surface grid used in discretizing the dielectric interface at the pore wall, and a snapshot of the eight structural oxygen anions (red) and two cations dwelling in the pore (green, Ca^{2+}; blue, Na^+). Ions are represented as charged hard spheres with crystal radii (in Å: Ca^{2+} 0.99; Ba^{2+} 1.35; Li^+ 0.6; Na^+ 0.95; K^+ 1.33; Cl^- 1.81; $O^{1/2-}$ 1.4).

on the concentrations of ions in the baths. Models or simulations (e.g., of molecular dynamics) that use only one concentration in the bath could not predict any of these phenomena. Computations done with a concentration of "zero"—implicitly assumed when infinitely dilute solutions are considered—would be at a particular disadvantage in describing these phenomena that depend on the variation of concentration in the baths in the domain where nonideal properties are important.

The average number of ions in the central 5-Å section of the pore provides an index of this selectivity for ion size (Fig. 3). The absorption curves for Na^+ and K^+ are similar to those for Ca^{2+} and Ba^{2+}. The effect of ion size on ion absorption thus does not substantially depend on ion valency, even though the valency has large effects on all electrostatic forces. (Electrostatic screening forces vary with the square of the valency.) We conclude that the size effect is not chiefly due to size-dependent electrostatic screening, but to a direct competition for space.

Concentration profiles like those of Fig. 2 can be used to predict slope conductance for a channel tested with a small driving force, so that simulation results and experimental conductances can be compared. Because our simulations do not include hydrogen ions, their comparison with experiment needs to be safeguarded against complications due to hydrogen ions. Calcium channel currents carried by 160 mM of alkali metal ions (except Li^+) are depressed by physiological amounts of hydrogen ion (Pietrobon et al., 1989), as if the glutamate groups of the EEEE locus are partially neutralized by protonation and thus attract less alkali metal counterion for conduction. The apparent pK_A for blockade of Na^+ current is 7.5 (Fig. 5 of Pietrobon et al., 1989). Our simulations with Na^+ thus can be compared with experiments performed at pH 9. Currents carried by 1.8 mM Ca^{2+} are not significantly reduced by lowering pH to 6.5 (Prod'hom et al., 1989), and currents carried by ≥50 mM Ba^{2+} appear to be saturated at pH ≥ 7.4 (Prod'hom et al., 1989; Kuo and Hess, 1993b; Klöckner and Isenberg, 1994). Simulations excluding hydrogen ions and using a total concentration of 50–100 mM for these divalent cations thus seem to be comparable to the published experimental conductances.

Comparisons of experimental and computed conduction are shown in Fig. 4. In one experiment, the extracellular mole fractions of Li^+ and Na^+ were varied at a

Published April 27, 2009

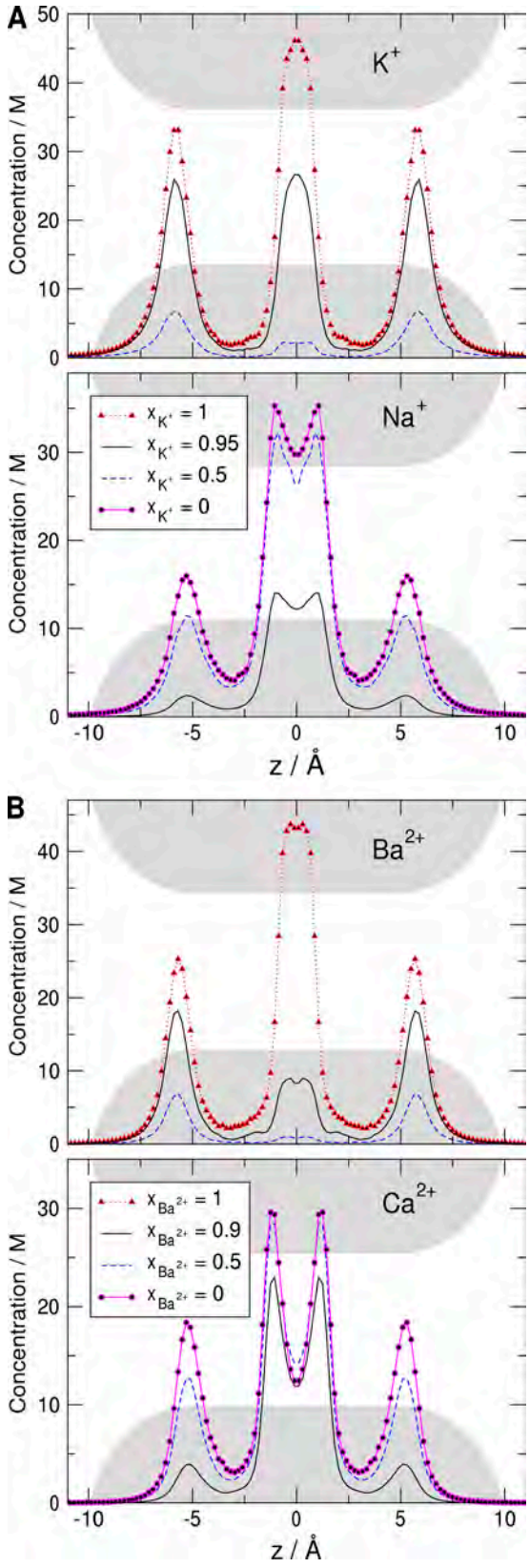

Figure 2. Competitive "binding" of ions of equal charges. Simulated distributions of ions in the axial pore dimension. The concentrations are average concentrations in subvolumes obtained by dividing the aqueous region into slices perpendicular to the pore axis. The bath contained either NaCl and KCl (A; total concentration, 0.1 M) or $CaCl_2$ and $BaCl_2$ (B; 0.05 M) in varied mole fractions, *x*.

maintained total concentration of 160 mM (Fig. 5 of Prod'hom et al., 1989). The "×" symbols in Fig. 4 A represent the experimental conductances, measured from the linear inward branch of current voltage relations of individual channels in on-cell membrane patches. We estimate the diffusion coefficients for Na^+ and Li^+ from the conductance values observed for Li^+ mole fractions of 0 and 1, and use the simulated concentration profiles to predict the mole-fraction effect on conductance for intermediate mole fractions between 0 and 1 (Fig. 4 A, filled circles and line). The pore model predicts the nonlinear relation observed between conductance and Li^+ mole fraction quite well.

In the second experiment, Ca^{2+} was added to an extracellular solution containing a fixed concentration of Ba^{2+} (50 mM). Inward single-channel currents recorded from on-cell membrane patches (Fig. 8 of Hess et al., 1986) are replotted as "×" symbols in our Fig. 4 B. The curve in Fig. 4 B is our prediction based on axial concentration profiles determined by simulations with symmetrical bath solutions. Diffusion coefficients for Ca^{2+} and Ba^{2+} were estimated from the conductances of 9 pS (Ca^{2+}) and 20 pS (Ba^{2+}) that were measured with external baths containing either one or the other (but not both) of the species (Hess et al., 1986). The simulation-based conductance curves have been scaled to give a current of 1.25 pA in 50 mM of pure Ba^{2+} saline. Again, the relation between experiment and prediction is qualitatively correct and quantitatively quite good.

Our model then predicts size-specific concentrations of cations in the calcium channel. When given a choice between two ion species of the same charge, the channel prefers small ions, in agreement with experiment. When extended by drift-diffusion theory (Eq. 3), the selective absorption of the model accounts for conduction phenomena experimentally observed when two ion species of the same charge compete for the L-type calcium channel. The CSC model provides a physical basis for these phenomena.

Selective absorption of cations with unequal charges

This section presents computations in mixed solutions now containing cations of unequal valencies. We show the competitive absorption of alkali metal ions and Ca^{2+} (or Ba^{2+}) in the model pore and compare these to experiment. The selectivity in this absorption is thought to be the basis of the physiological selectivity of the L-type calcium channel, which conducts Ca^{2+} in preference to Na^+ and K^+, even though these alkali metal ions are present in physiological solutions in hundredfold larger concentration than Ca^{2+}. In our model, which represents ions as charged hard spheres, Na^+ and Ca^{2+}

Published April 27, 2009

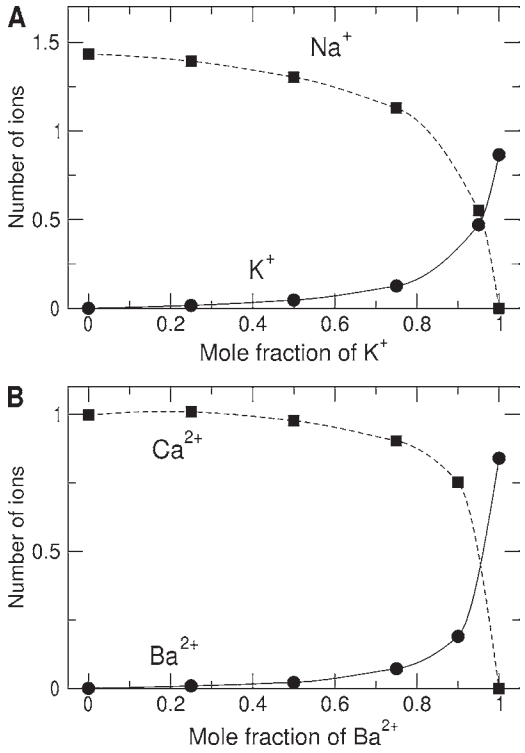

Figure 3. Competitive "binding" of ions of equal charges. Average numbers of ions of a species present in the central region of the pore ($-2.5 < z/\text{Å} < 2.5$). From the same simulations as Fig. 2.

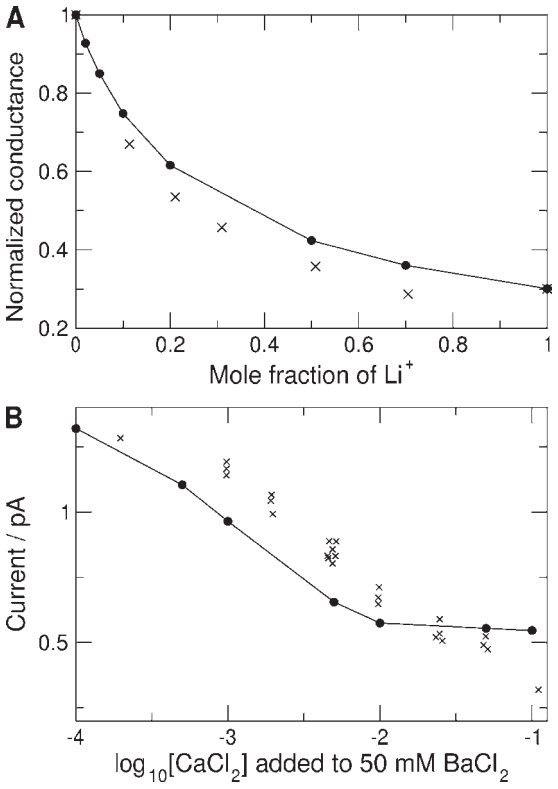

Figure 4. Competitive conduction of ions of equal charges: comparison to experiment. (A) Varied mole fraction in mixed solutions of LiCl and NaCl (total concentration, 0.16 M). (B) 0.05 M $BaCl_2$ solution with varied amount of added $CaCl_2$. The filled circles and lines represent pore conductances computed from Eq. 3 using simulated axial number densities of the ions. The "×" symbols represent experimental results.

have almost equal (crystal) radii. Their only distinguishing property is charge.

We compute the competition of Na^+ and Ca^{2+} under conditions approximating those of the classical experiment of Almers et al. (1984). These workers used external solutions containing the fixed Na^+ concentration of 32 mM and a variable concentration of Ca^{2+}; the intracellular solution of the frog skeletal muscle fibers contained 32 mM Cs^+. All solutions were made isotonic by including a salt of a (presumably) "inert" organic cation. Sub-millimolar concentrations of "free" Ca^{2+} were buffered with various calcium chelators. All solutions contained pH buffer and were adjusted for pH 7. Our equilibrium simulations are restricted to symmetrical bath compositions. We establish a controlled bulk concentration of Ca^{2+} by imposing an appropriate chemical potential for $CaCl_2$ in the grand canonical ensemble. Simulations of very small Ca^{2+} concentrations can be made this way. Our simulations do not include protons.

Fig. 5 shows profiles of concentration along the axis of the channel computed for baths containing 30 mM Na^+ and a varied amount of Ca^{2+}. These profiles are basically similar in shape to those already described for Na^+ and Ca^{2+} (compare Fig. 2), but a very small Ca^{2+} concentration, ~1 μM, is enough to establish similar concentrations of Na^+ and Ca^{2+} in the central part of the pore. This part of model pore absorbs Ca^{2+} with strong selectivity over Na^+.

The numbers of Na^+ and Ca^{2+} absorbed in the central 5-Å section of the pore are plotted in Fig. 6 A (closed symbols). The curves are first-order binding curves fitted to the simulation results with mixed solutions (closed symbols) and the simulation result for Ca^{2+}-free baths (not depicted). The Ca^{2+} concentration that displaces one half the Na^+ ions from the pore center is close to 1 μM. When Almers et al. (1984) fitted such a binding curve to their experimental results, they found that 0.7 μM of external Ca^{2+} reduced Na^+ current by one half.

Our reduced physical model produces a Ca^{2+}/Na^+ selectivity comparable to that of the biological channel. It thus can in principle account for the pivotal observation on calcium channel selectivity, even though the model includes no high-affinity binding site preformed by a specific atomic structure nor interactions beyond those of hard-sphere ions. The self-organized induced fit of structural ions and permeating ions is enough to predict the main biological phenomena if care is taken to compute structures at equilibrium with positions that can vary as the concentration and species of ions in the baths are varied.

The concentration profiles that we show in Fig. 5, when combined with Eq. 3, predict the well-known

Published April 27, 2009

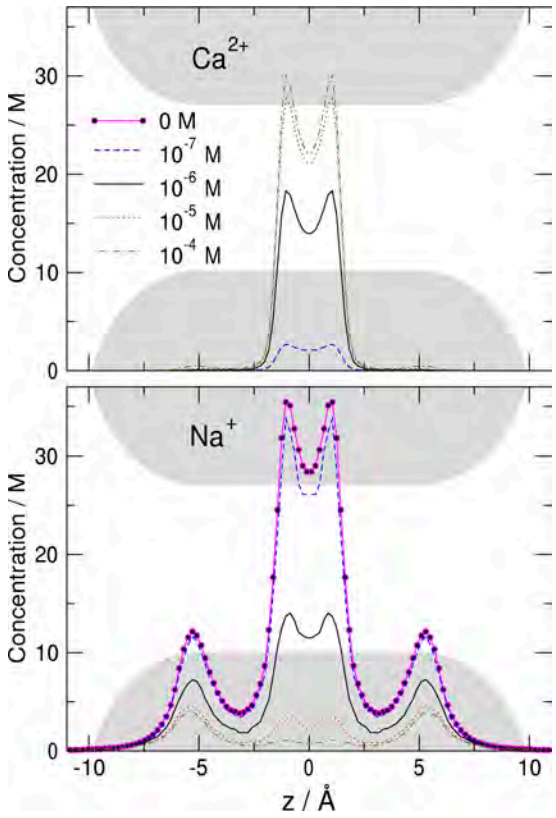

Figure 5. Competitive "binding" of Ca^{2+} and Na^+. Simulated distributions of ions in the axial pore dimension. A varied amount of $CaCl_2$ was added to a fixed concentration of NaCl (0.03 M).

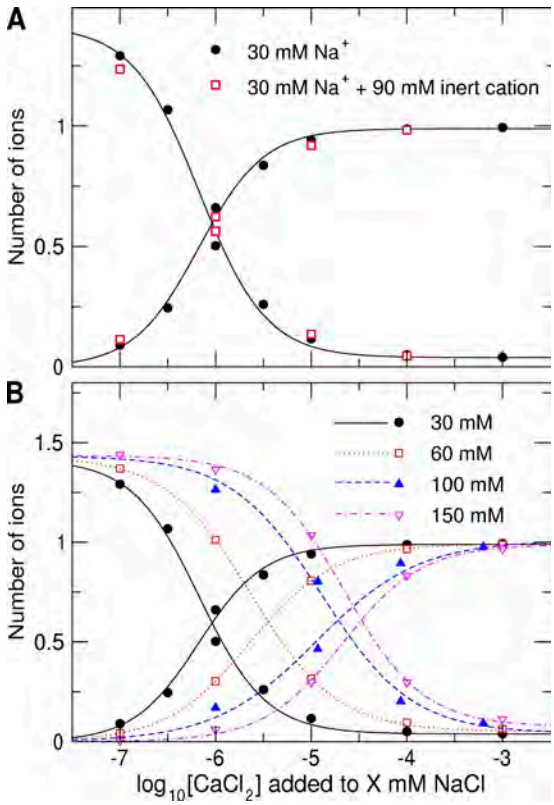

Figure 6. Competitive "binding" of Ca^{2+} and Na^+. Average numbers of Ca^{2+} (increasing curves) and Na^+ (decreasing curves) absorbed into the central region of the pore. (A) $CaCl_2$ added to 0.03 M NaCl (closed symbols) or to 0.03 M NaCl + 0.09 M MCl (M^+ is a "large" cation of radius 2.5 Å). (B) Varied amounts of $CaCl_2$ added to baths containing different fixed concentrations of NaCl.

anomalous mole fraction behavior in Na^+/Ca^{2+} mixed solutions, as discussed in detail previously (Gillespie et al., 2008; Gillespie and Boda, 2008).

Various other conditions involving ions of different charges were examined. We made simulations with added "inert" cations, with varied Na^+ concentration, or with varied species of alkali or alkaline earth metal ions.

To mimic the "inert" salt that was present in the solutions of Almers et al. (1984), we include, besides 30 mM NaCl, 90 mM of the chloride salt of a large cation (radius 2.5 Å). Simulation results for this condition (Fig. 6 A, open symbols) superimpose on those done with only 30 mM NaCl in the baths (closed symbols). Indeed, a large monovalent cation acts as inert cation in the model.

Variation of the concentration of the sodium salt biases Na^+/Ca^{2+} competition in the model pore. Na^+/Ca^{2+} exchange characteristics computed for Na^+ bath concentrations of 30, 60, 100, and 150 mM are superimposed in Fig. 6 B. As Na^+ concentration increases in the baths, a larger Ca^{2+} concentration is needed to displace Na^+ from the central pore region. Experiments performed in different laboratories have tested the blockade of inward Na^+ current by micromolar free Ca^{2+} at extracellular Na^+ concentrations of ≈30, 150, or 200 mM Na^+. Consistently, half-blockade of inward sodium current was found for a small Ca^{2+} concentration, on the order of 1 μM (Kostyuk et al., 1983; Almers et al., 1984; Hess and Tsien, 1984; Rosenberg and Chen, 1991), as if variation of extracellular Na^+ concentration in this range does not bias affinity for Ca^{2+} in L-type channels. On the other hand, a study by Kuo and Hess (1993b) found that an increase of Na^+ concentration from 0.1 to 0.3 M (on both sides of the channel) reduces the probability of blockade of Na^+ outward current by 3.5 μM of extracellular Ca^{2+} about twofold (their Fig. 4). An assessment of the role of Na^+ in Ca^{2+} blockade needs to consider that solutions of different concentrations were applied symmetrically in some experiments but asymmetrically in others (with a different concentration of Na^+ or a different monovalent cation on the other side), in conjunction with different, symmetrical or asymmetrical, proton concentrations (pH range of 7.0 to 9.0), with free Ca^{2+} concentrations established using different Ca^{2+} buffers in different backgrounds of 1:1 salts and different approaches to compute the composition required to establish the free Ca^{2+} concentrations. On the other hand, we simulate symmetrical, proton-free ionic conditions with unambiguously known Ca^{2+} concentrations.

The species of the alkali metal ion is also important in the competition with Ca^{2+} for the model pore (Fig. 7 A).

Published April 27, 2009

The bath concentration of Ca^{2+} required to displace half the monovalent cation from the pore increases substantially as the species of ion is changed from K^+ to Li^+. When the bath contains the pure alkali metal salt (100 mM), the average number of cations in the central region of the pore increases as the ion radius of the cation species decreases (compare also Fig. 3 A). The blockade of Li^+-carried currents by Ca^{2+} has been investigated in L-type calcium channels (Lansman et al., 1986; Kuo and Hess, 1993a,b). The blockade occurred at Ca^{2+} concentrations of the order of 1 μM, which appears to differ from the results of our simulations.

The experimental results reported with different species or concentrations of alkali metal ion appear to be inconsistent with a mechanism based on competition of monovalent cations with Ca^{2+}. Competition implies that both the species and concentration of the monovalent cation(s) contribute to the balance. Our model produces these competitive dependencies; the experiments do not. The issue here is not just the disagreement between model and experiment. At issue here is also why the experiments do not show the qualitative characteristics of the competitive mechanism that is commonly thought to determine selectivity in calcium channels.

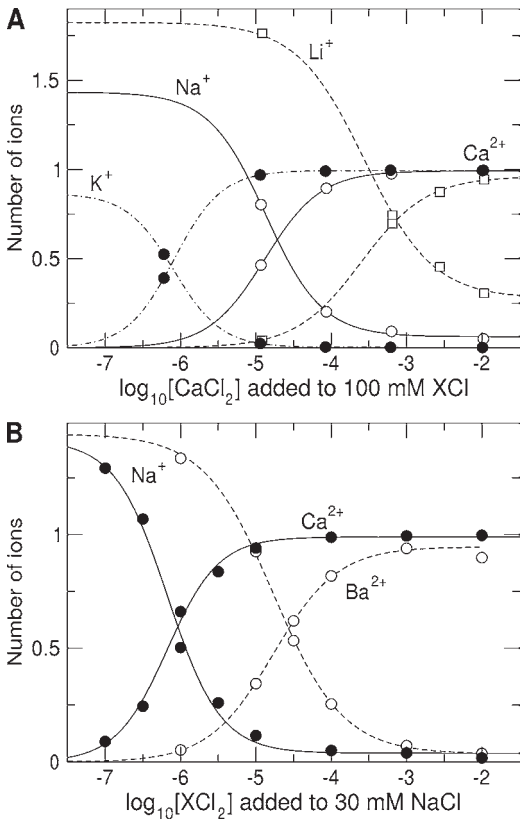

Figure 7. Competitive ion "binding": effect of species of monovalent (A) or divalent cation (B). Average numbers of cations of a species present in the central region of the pore. (A) $CaCl_2$ added to 0.1 M LiCl, NaCl, or KCl. (B) $CaCl_2$ or $BaCl_2$ added to 0.03 M NaCl.

The existence of a competitive mechanism is strongly supported by a different class of experiments: time-resolved measurements of the blockade of Li^+ currents by Ca^{2+} in L-type calcium channels (Kuo and Hess, 1993a,b). These experiments (discussed in the subsequent section of this paper) indicated species-specific and concentration-dependent effects of Li^+ on the kinetics of the Ca^{2+} blockade that locate the blocking Ca^{2+} to the pore.

We suggest that the independence (of Ca^{2+} blockade on alkali metal background) is an artifact produced by a questionable method of estimating "free" Ca^{2+} concentration in experiments using calcium buffers (see Discussion). In particular, the concentration of free Ca^{2+} was computed assuming that each type of alkali metal ion has the same effect on free Ca^{2+} concentrations. If this assumption does not hold, the reported experimental results represent only the difference between properties of the binding site of the calcium chelator and the binding site of the channel. If the chelator binding varies with ion type, but this variation is not included in the analysis of the chelator, the variation of binding in the channel with ion type will not be seen in the results.

We have also simulated an experiment of Kostyuk et al. (1983), who compared blockades of Na^+ current by various divalent cations. Fig. 7 B shows simulation results for the number of Ba^{2+} ions in the central region of the pore, together with results for Ca^{2+} shown earlier (Fig. 6). The bath contained a fixed concentration of Na^+ (30 mM). The divalent cation concentration required to displace one half the Na^+ from the region is much larger for Ba^{2+} than for Ca^{2+}, a shift similar to that observed in the blockade experiments of Kostyuk et al. (1983) (their Fig. 8). Our model thus reproduces the experimental pattern. The solutions used in these experiments were made with a Ca^{2+} buffer, but the concentration or species of the alkali metal cation were not varied in this case, and so artifacts of the type just described would not occur.

Ca^{2+} entry/exit rates depend on the concentration of Li^+

Discrete fluctuations observed in currents carried by Li^+ in the presence of micromolar Ca^{2+} are thought to occur when individual Ca^{2+} ions enter and leave the L-type calcium channel (Kuo and Hess, 1993a). Variations of extracellular or intracellular Li^+ concentrations modulate the rates at which a Ca^{2+} appears to enter or leave the pore (Kuo and Hess, 1993b). For example, increasing Li^+ concentration on the side opposite to that of Ca^{2+} appears to slow the exit rate of a Ca^{2+} dwelling in the pore, and increasing Li^+ concentration on the side of Ca^{2+} application appears to both reduce the rate of Ca^{2+} entry and increase the rate of Ca^{2+} exit, thereby reducing the overall extent of the blockade. A study on N-type calcium channels has revealed a reduction of divalent

Published April 27, 2009

ion current associated with an increase of extracellular Na^+ concentration (Polo-Parada and Korn, 1997). Chemical kinetics descriptions including "high-affinity binding sites" flanked by "low-affinity sites" and a conduction mechanism based on vacancy hopping in a queue have been made to explain these phenomena.

We have simulated bath ionic conditions involving micromolar Ca^{2+} and a varied background of Li^+ in our model to determine how Li^+ affects the average Ca^{2+} distribution along the model pore (Fig. 8). A simulation with a bath containing 0.05 M Li^+ and 10^{-4} M Ca^{2+} yields a Ca^{2+} distribution with two large concentration maxima near the center of the pore that are flanked by two small maxima located near the mouths of the pore (dashed line in Fig. 8 A; compare also Figs. 2 B and 5).

The computed pattern of Ca^{2+} distribution is indeed similar to that implied by one of the proposed chemical kinetics descriptions (Dang and McCleskey, 1998): the pore forms two closely spaced high-affinity regions for Ca^{2+} near its center and two low-affinity regions in its periphery. The high-affinity region accepts no more than one Ca^{2+} (see also Figs. 6 and 7). This pattern arises naturally from the force fields that we have included into the reduced model of the EEEE locus.

In a simulation with a larger concentration of Li^+ in the bath (0.3 M; solid line in Fig. 8) Ca^{2+}, concentration is less in all regions of the pore compared with the simulation with 0.05 M Li^+, whereas the concentration of Li^+ in the pore is larger (Fig. 8 B). Specifically, the average number of Li^+ ions dwelling in the axial region between $z = -7$ Å and $z = -3$ Å (one of the "low-affinity sites") increases from 0.44 to 0.85 when the bath concentration of Li^+ is varied from 0.05 to 0.3 M. Thus, a Ca^{2+} exit rate depending on a vacant low-affinity site might be expected to decrease.

Our MC simulations cannot study asymmetrical ionic conditions like those investigated by Kuo and Hess (1993b). Insight into Ca^{2+} diffusion under symmetrical conditions, however, can be gained by incorporating equilibrium ion concentrations computed by simulation into a drift-diffusion description of ion motion (Eq. 3). Because we do not restrict diffusion to vacancy hopping in a queue, in this computation we can assess factors affecting Ca^{2+} transport not depending on restricted diffusion. The calculation predicts that the Ca^{2+} conduction rate is reduced 11.5-fold by raising the Li^+ concentration of the bath from 0.05 to 0.3 M. The factor crucial for Ca^{2+} passage in the model is the likelihood of Ca^{2+}-accessing pore regions where Ca^{2+} is least likely to dwell ("energy barriers" in the language of chemical kinetics descriptions; "depletion zones" in the language of self-consistent models) (Selberherr, 1984; Nonner et al., 1998; Eisenberg, 2005, 1996b; Gillespie and Boda, 2008).

Two such regions are symmetrically located on either side of the central region where Ca^{2+} is most likely to dwell (Fig. 8 A). The local Ca^{2+} concentration in these two regions (and thus the height of the barrier) are highly sensitive to Li^+ concentration in the bath. Such dependency of a barrier on bath composition has not been envisaged in chemical kinetics descriptions. In our simulations, the axial regions depleted of Ca^{2+} co-locate with the largest densities of the structural oxygen ions (Fig. 8 C). Ca^{2+} dwelling in one of these regions involves a thermodynamically unfavorable packing of Ca^{2+} and counterions because the restricted oxygen anions screen a Ca^{2+} dwelling in this location less effectively than a more centrally located Ca^{2+}. They tend to exclude Ca^{2+} or other ions due to their finite volume. A high concentration of Li^+ in the baths results in deeper depletion (or a higher barrier). Vacancy hopping in a queue is not required for this kind of Li^+ action.

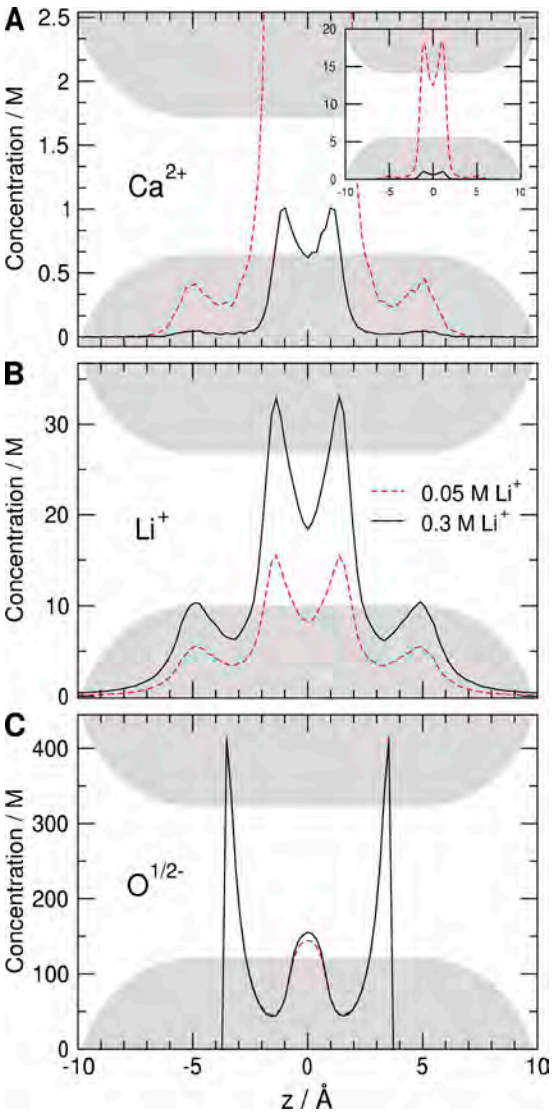

Figure 8. Ca^{2+} distribution in the pore modulated by variation of LiCl concentration. Simulated distributions of ions (Ca^{2+}, Li^+, and $O^{1/2-}$ in A, B, and C, respectively) in the axial dimension. The bath contained 10^{-4} M $CaCl_2$ and either 0.05 or 0.3 M LiCl.

Published April 27, 2009

DISCUSSION

We have made a physical model of selective "ion binding" in the L-type calcium channel and have compared consequences of the model with experimental data. Our model is reduced, treating only ions and the carboxylate oxygens of the EEEE locus explicitly and restricting interactions to hard-core repulsion and ion–ion and ion–dielectric electrostatic forces. We have compared simulation results to a variety of experimental observations made with bath solutions containing binary mixtures of alkali and/or alkaline earth metal ions.

The model pore produces the biologically relevant selectivity of L-type (and other) calcium channels: alkali metal cations are rejected in the presence of physiological concentrations of Ca^{2+}. Specifically, the model predicts the blockade of currents carried by alkali metal ions observed in experiments at low micromolar concentrations of Ca^{2+}. The model also predicts conductance patterns observed in varied mixtures containing two species of alkali metal ion (including Li^+ and Na^+) or Ba^{2+} and Ca^{2+}. In the blockade of monovalent ion current by micromolar amounts of divalent cations, a substantial difference in blocking potency observed between Ca^{2+} and Ba^{2+} is predicted.

Computed predictions and experiment appear to differ in the case of Ca^{2+} actions on currents carried by different species of alkali metal cation or different concentrations of these cations. Here, the model predicts strong difference between the currents carried by different alkali metal ions, as does any model in which competition arises between different species, but the experiments show virtually none. On the other hand, the model predicts effects of Li^+ concentration that are consistent with observed time resolved measurements of the kinetics of Ca^{2+} association and dissociation in Li^+ solutions. In contrast to the experiments on Ca^{2+} blockade of L-type calcium channels, the experimental results obtained for proton blockade of the channels show strong alkali metal dependence of the block (Pietrobon et al., 1989; Prod'hom et al., 1989).

The "free" Ca^{2+} concentrations of the solutions used in the experiments that our model does not reproduce were buffered by Ca^{2+} chelators. However, these "free" Ca^{2+} concentrations in the experimental work were not measured. They were calculated using a heuristic description of Ca^{2+} binding by the chelator (a sequence of covalent chemical reactions described by mass action law, with reactants described by concentrations). The term "free concentration" has no physical meaning beyond that implied by this heuristic model of Ca^{2+} buffering. Calibrated measurements of Ca^{2+} activity in each experimental solution would be a great help.

The physics included in our reduced model of the EEEE locus also operate in a chelator that involves carboxylate anions tethered into a cluster. Our self-consistent simulations show that the physics by which Ca^{2+} and alkali metal ions interact with a cluster of confined oxygen anions give properties not anticipated in the heuristic equations of Ca^{2+} buffering. If chelators have properties similar to our channel model, and the chelators thus respond differently to different species or concentrations of alkali metal ions, the experiments will only report the differences in the potencies of Ca^{2+} binding between chelator and channel.

If the dependence of chelator binding on the species of alkali metal ion is ignored, the experiments seem to show binding by the channel that is independent of alkali metal species. A channel like this does not show competitive binding at all. Indeed, it cannot be described by a simple law of mass action for competitive Ca^{2+} binding. Given this situation, it is probably most constructive to view our computational results for dependence of Ca^{2+} blockade on the alkali metals as a prediction and look forward to experimental tests of these predictions, in which the activity of Ca^{2+} is measured as alkali metal ions are changed in species or amount.

Summary and conclusion

Here, we have presented a reduced physical model of the EEEE locus. The model is reduced to a small group of atoms and two kinds of force that are treated explicitly. Using a reductionist approach, we sought to determine how much of the system needs to be modeled in atomic detail and what kinds of interatomic interactions are crucial for the ionic selectivity of biological interest. The results of the reduced model, as described, are surprisingly realistic, particularly if one considers how much has been treated at low resolution or has been left out.

Our results then let us propose a mechanism of selectivity based on the cooperation of two forces that are certainly involved in any crowded selectivity filter: (1) the net charges of the acidic groups of the EEEE locus tend to attract equivalent amounts of cations into the small volume of the selectivity filter. This long-range attraction in itself favors divalent over monovalent cations, so that, e.g., Ca^{2+} is preferred over Na^+. (2) The resulting local density of ions in the selectivity filter, tens of moles, brings to bear the hard-core repulsion among atoms. This force has the strongest dependence on interatomic distance of all interatomic forces. It limits the closest approach of ions in the filter and thus their close-range electrostatic interactions, favoring small ions. Furthermore, ions with large radii are less likely to find an adequate cavity in the dense particle ensemble of the selectivity filter. This entropic contribution increases very strongly with the particle density and thus by itself can produce a large amount of size selectivity. This system selects for the cation that can deliver the largest charge in the smallest ion volume.

A reduced physical model thus produces selectivity comparable to that of the biological channel, even though

Published April 27, 2009

the model includes no preformed binding sites or interactions beyond those of hard-sphere ions. The self-organized induced fit of structural ions and permeating ions is enough to predict the main biological phenomena, if care is taken to compute structures at equilibrium with positions and "flexibility" that can vary as the concentration and species of ions in the baths are varied.

A generous allotment of computer time by the Ira and Marylou Fulton Supercomputing Center at Brigham Young University is acknowledged with thanks.

The authors are grateful for the support of the Hungarian National Research Fund (OTKA K63322 to D. Boda and OTKA K68641 to M. Valiskó), National Institutes of Health (grants GM067241 to B. Eisenberg and GM083161 to W. Nonner), and a János Bolyai Research Fellowship (to M. Valiskó).

Edward N. Pugh Jr. served as editor.

Submitted: 29 January 2009
Accepted: 9 April 2009

REFERENCES

Almers, W., and E. McCleskey. 1984. Non-selective conductance in calcium channels of frog muscle: calcium selectivity in a single-file pore. *J. Physiol.* 353:585–608.

Almers, W., E. McCleskey, and P. Palade. 1984. Non-selective cation conductance in frog muscle membrane blocked by micromolar external calcium ions. *J. Physiol.* 353:565–583.

Boda, D., D. Busath, D. Henderson, and S. Sokołowski. 2000. Monte Carlo simulations of the mechanism of channel selectivity: the competition between volume exclusion and charge neutrality. *J. Phys. Chem. B.* 104:8903–8910.

Boda, D., D. Henderson, and D.D. Busath. 2001. Monte Carlo study of the effect of ion and channel size on the selectivity of a model calcium channel. *J. Phys. Chem. B.* 105:11574–11577.

Boda, D., D. Busath, B. Eisenberg, D. Henderson, and W. Nonner. 2002a. Monte Carlo simulations of ion selectivity in a biological Na^+ channel: charge-space competition. *Phys. Chem. Chem. Phys.* 4:5154–5160.

Boda, D., D. Henderson, and D. Busath. 2002b. Monte Carlo study of the selectivity of calcium channels: improved geometrical model. *Mol. Phys.* 100:2361–2368.

Boda, D., D. Gillespie, W. Nonner, D. Henderson, and B. Eisenberg. 2004. Computing induced charges in inhomogeneous dielectric media: application in a Monte Carlo simulation of complex ionic systems. *Phys. Rev. E Stat. Nonlin. Soft Matter Phys.* 69:046702.

Boda, D., M. Valiskó, B. Eisenberg, W. Nonner, D. Henderson, and D. Gillespie. 2006. Effect of protein dielectric coefficient on the ionic selectivity of a calcium channel. *J. Chem. Phys.* 125:34901.

Boda, D., W. Nonner, M. Valiskó, D. Henderson, B. Eisenberg, and D. Gillespie. 2007a. Steric selectivity in Na channels arising from protein polarization and mobile side chains. *Biophys. J.* 93:1960–1980.

Boda, D., M. Valiskó, B. Eisenberg, W. Nonner, D. Henderson, and D. Gillespie. 2007b. The combined effect of pore radius and protein dielectric coefficient on the selectivity of a calcium channel. *Phys. Rev. Lett.* 98:168102.

Boda, D., W. Nonner, D. Henderson, B. Eisenberg, and D. Gillespie. 2008. Volume exclusion in calcium selective channels. *Biophys. J.* 94:3486–3496.

Chen, X.H., I. Bezprozvanny, and R. Tsien. 1996. Molecular basis of proton block of L-type Ca^{2+} channels. *J. Gen. Physiol.* 108:363–374.

Corry, B., T.B. Allen, S. Kuyucak, and S.H. Chung. 2001. Mechanisms of permeation and selectivity in calcium channels. *Biophys. J.* 80:195–214.

Dang, T.X., and E.W. McCleskey. 1998. Ion channel selectivity through stepwise changes in binding affinity. *J. Gen. Physiol.* 111:185–193.

Dudev, T., and C. Lim. 2004. Monodentate versus bidentate carboxylate binding in magnesium and calcium proteins: what are the basic principles? *J. Phys. Chem. B.* 108:4546–4557.

Eisenberg, B. 2005. Living transistors: a physicist's view of ion channels. Version 2. http://arxiv.org/abs/q-bio/0506016 (accessed April 17, 2009).

Eisenberg, R.S. 1996a. Atomic Biology, Electrostatics and Ionic Channels. New Developments and Theoretical Studies of Proteins. Volume 7. 269–357. World Scientific, Philadelphia. Also available at http://arxiv.org/abs/0807.0715 (accessed April 17, 2009).

Eisenberg, R.S. 1996b. Computing the field in proteins and channels. *J. Membr. Biol.* 150:1–25.

Ellinor, P.T., J. Yang, W.A. Sather, J.-F. Zhang, and R. Tsien. 1995. Ca^{2+} channel selectivity at a single locus for high-affinity Ca^{2+} interactions. *Neuron.* 15:1121–1132.

Fenwick, E.M., A. Marty, and E. Neher. 1982. Sodium and calcium channels in bovine chromaffine cells. *J. Physiol.* 331:599–635.

Friel, D.D., and R.W. Tsien. 1989. Voltage-gated calcium channels: direct observation of the anomalous mole fraction effect at the single-channel level. *Proc. Natl. Acad. Sci. USA.* 86:5207–5211.

Gillespie, D. 2008. Energetics of divalent selectivity in a calcium channel: the ryanodine receptor case study. *Biophys. J.* 94:1169–1184.

Gillespie, D., and D. Boda. 2008. The anomalous mole fraction effect in calcium channels: a measure of preferential selectivity. *Biophys. J.* 95:2658–2672.

Gillespie, D., W. Nonner, and B. Eisenberg. 2002. Coupling Poisson-Nernst-Planck and density function theory to calculate ion flux. *J. Phys. Condens. Matter.* 14:12129–12145.

Gillespie, D., L. Xu, Y. Wang, and G. Meissner. 2005. (De)constructing the ryanodine receptor: modeling ion permeation and selectivity of the calcium release channel. *J. Phys. Chem. B.* 109:15598–15610.

Gillespie, D., D. Boda, Y. He, P. Apel, and Z.S. Siwy. 2008. Synthetic nanopores as a test case for ion channel theories: the anomalous mole fraction effect without single filing. *Biophys. J.* 95:609–619.

Hagiwara, S. 1983. Membrane Potential-Dependent Ion Channels in Cell Membranes. Raven Press, New York. 118 pp.

Henderson, D. 2009. Attractive energy and entropy or particle size: the yin and yang of physical and biological science. *Interdiscip. Sci. Comput. Life Sci.* 1:1–11. Also available at http://arxiv.org/abs/0904.0991v1 (accessed April 17, 2009).

Hess, P., and R. Tsien. 1984. Mechanism of ion permeation through calcium channels. *Nature.* 309:453–456.

Hess, P., J. Lansman, and R. Tsien. 1986. Calcium channel selectivity for divalent and monovalent cations. Voltage and concentration dependence of single channel current in ventricular heart cells. *J. Gen. Physiol.* 88:293–319.

Hille, B. 2001. Ionic Channels of Excitable Membranes. Sinauer Associates, Sunderland, MA. 814 pp.

Jacoboni, C., and P. Lugli. 1989. The Monte Carlo Method for Semiconductor Device Simulation. Springer-Verlag, New York. 356 pp.

Klöckner, U., and G. Isenberg. 1994. Calcium channel current of vascular smooth muscle cells: extracellular protons modulate gating and single channel conductance. *J. Gen. Physiol.* 103:665–678.

Koch, S.E., I. Bodi, A. Schwartz, and G. Varadi. 2000. Architecture of Ca^{2+} channel pore-lining segments revealed by covalent modification of substituted cysteines. *J. Biol. Chem.* 275:34493–34500.

Kostyuk, P.G., S.L. Mironov, and Y.M. Shuba. 1983. Two ion-selective filters in the calcium channel of the somatic membrane of mollusk neurons. *J. Membr. Biol.* 76:83–93.

Published April 27, 2009

Kuo, C.C., and P. Hess. 1993a. Ion permeation through the L-type Ca^{2+} channel in rat phaeochromocytoma cells: two sets of ion binding sites in the pore. *J. Physiol.* 466:629–655.

Kuo, C.C., and P. Hess. 1993b. Characterization of the high-affinity Ca^{2+} binding sites in the L-type Ca^{2+} channel pore in rat phaeochromacytoma cells. *J. Physiol.* 466:657–682.

Lansman, J.B., P. Hess, and R. Tsien. 1986. Blockade of current through single calcium channels by Cd^{2+}, Mg^{2+}, and Ca^{2+}. Voltage and concentration dependence of calcium entry into the pore. *J. Gen. Physiol.* 88:321–347.

Lee, K.S., and R. Tsien. 1984. High selectivity of calcium channels in single dialysed heart cells of the guinea pig. *J. Physiol.* 354:253–272.

Lundstrom, M. 2000. Fundamentals of Carrier Transport. Addison-Wesley, New York. 418 pp.

Malasics, A., D. Gillespie, and D. Boda. 2008. Simulating prescribed particle densities in the grand canonical ensemble using iterative algorithms. *J. Chem. Phys.* 128:124102.

Nonner, W., D.P. Chen, and B. Eisenberg. 1998. Anomalous mole fraction effect, electrostatics, and binding in ionic channels. *Biophys. J.* 74:2327–2334.

Nonner, W., L. Catacuzzeno, and B. Eisenberg. 2000. Binding and selectivity in L-type Ca channels: a mean spherical approximation. *Biophys. J.* 79:1976–1992.

Nonner, W., D. Gillespie, D. Henderson, and B. Eisenberg. 2001. Ion accumulation in a biological calcium channel: effects of solvent and confining pressure. *J. Phys. Chem. B.* 105:6427–6436.

Noskov, S.Y., and B. Roux. 2007. Importance of hydration and dynamics on the selectivity of the KcsA and NaK channels. *J. Gen. Physiol.* 129:135–143.

Pietrobon, D., B. Prod'hom, and P. Hess. 1988. Conformational changes associated with ion permeation in L-type calcium channels. *Nature.* 323:373–376.

Pietrobon, D., B. Prod'hom, and P. Hess. 1989. Interactions of protons with single open L-type calcium channels. pH dependence of proton-induced current fluctuations with Ca^{+}, K^{+}, and Na^{+} as permeant ions. *J. Gen. Physiol.* 94:1–21.

Polo-Parada, L., and S.J. Korn. 1997. Block of N-type calcium channels in chick sensory neurons by external sodium. *J. Gen. Physiol.* 109:693–702.

Prod'hom, B., D. Pietrobon, and P. Hess. 1989. Interactions of protons with single open L-type calcium channels. Location of protonation site and dependence of proton-induced current fluctuations on concentration and species of permeant ion. *J. Gen. Physiol.* 94:23–42.

Reuter, H., and H. Scholz. 1977. A study of the ion selectivity and the kinetic properties of the calcium dependent slow inward current in mammalian cardiac muscle. *J. Physiol.* 264:17–47.

Rosenberg, R.L., and X. Chen. 1991. Characterization and localization of two ion-binding sites within the pore of cardiac L-type calcium channels. *J. Gen. Physiol.* 97:1207–1225.

Sather, W.A., and W. McCleskey. 2003. Permeation and selectivity in calcium channels. *Annu. Rev. Physiol.* 65:133–159.

Selberherr, S. 1984. Analysis and Simulation of Semiconductor Devices. Springer-Verlag, New York. 293 pp.

Valleau, J.P., and L.K. Cohen. 1980. Primitive model electrolytes. I. Grand canonical Monte Carlo computations. *J. Chem. Phys.* 72:5935–5941.

Yang, J., P.T. Ellinor, W.A. Sather, J.F. Zhang, and R. Tsien. 1993. Molecular determinants of Ca^{2+} selectivity and ion permeation in L-type Ca^{2+} channels. *Nature.* 366:158–161.

Yue, D.T., and E. Marban. 1990. Permeation in the dihydropyridine-sensitive calcium channel. Multi-ion occupancy but no anomalous mole-fraction effect between Ba^{2+} and Ca^{2+}. *J. Gen. Physiol.* 95:911–939.